Available online at www.sciencedirect.com
ScienceDirect
Renewable Energy 33 (2008) 2134–2144
RENEWABLE ENERGY
www.elsevier.com/locate/renene

Technical Note

Performance optimization of Stirling engines

Youssef Timoumi*, Iskander Tlili, Sassi Ben Nasrallah

Laboratoire d'Etude des Systèmes Thermiques et Energétiques, Ecole Nationale d'Ingénieurs de Monastir, Rue Ibn El Jazzar, 5019 Monastir, Tunisie

Received 1 June 2007; accepted 16 December 2007
Available online 13 February 2008

Abstract

The search for an engine cycle with high efficiency, multi-sources of energy and less pollution has led to reconsideration of the Stirling cycle. Several engine prototypes were designed but their performances remain relatively weak when compared with other types of combustion engines. In order to increase their performances and analyze their operations, a numerical simulation model taking into account thermal losses has been developed and used, in this paper, to optimize the engine performance. This model has been tested using the experimental data obtained from the General Motor GPU-3 Stirling engine prototype. A good correlation between experimental data and model prediction has been found. The model has also been used to investigate the influence of geometrical and physical parameters on the Stirling engine performance and to determine the optimal parameters for an acceptable operational gas pressure.
© 2007 Elsevier Ltd. All rights reserved.

Keywords: Stirling engines; Performance; Losses; Dynamic model; Regenerator; Thermal efficiency

1. Introduction

The urgent need to preserve fossil fuels and use renewable energies has led to the use of Stirling engines, which have an excellent theoretical efficiency, equivalent to the Carnot one. They can use any source of energy (combustion energy, solar energy…) and they are less polluting than the traditional engines.

Several prototypes were produced, Fig. 1, but their outputs remain very weak compared to the excellent theoretical yield, [1–5]. In fact, these engines have extremely complex phenomena related to the compressible fluid mechanics, thermodynamics, and heat transfer. An accurate description and understanding of these highly non-stationary phenomena is necessary so that different engine losses, optimal performance and design parameters can be determined.

Many investigators have studied the effect of some heat losses and irreversibilities on the engine performance indices. However, they have not calculated the optimal performance and design parameters for maximum power and efficiency. Popescu et al. [6] show that the most significant reduction in performance is due to the non-adiabatic regenerator. Kaushik, Wu and co-workers [7,8] have found that heat conductance between the engine and the reservoirs, the imperfect regenerator coefficient and the rates of the two regenerating processes are the important factors affecting the performance of a Stirling engine. Kongtragool and Wongwises [9] investigated the effect of regenerator effectiveness and dead volume on the engine network, heat input and efficiency by using a theoretical investigation on the thermodynamic analysis of a Stirling engine. Costea et al. [10] studied the effect of irreversibility on solar Stirling engine cycle performance; they included the effects of incomplete heat regeneration, internal and external irreversibility of the cycle as pressure losses due to fluid friction internal to the engine and mechanical friction between the moving parts. Cun-quan et al. [11] have established a dynamic simulation of an one-stage Oxford split-Stirling cryocooler. The regenerator inefficiency loss, the solid conduction loss, the shuttle loss, the pump loss and radiation loss are integrated into the mathematical model. The regenerator inefficiency loss and solid conduction loss are the most important. An acceptable agreement between experiment and simulation has been achieved. Cinar et al. [12] manufactured a beta-type Stirling engine operating at atmospheric pressure. The engine test

*Corresponding author. Tel.: +216 98 67 62 54; fax: +216 73 50 05 14.
E-mail address: Youssef.Timoumi@enim.rnu.tn (Y. Timoumi).

0960-1481/$ - see front matter © 2007 Elsevier Ltd. All rights reserved.
doi:10.1016/j.renene.2007.12.012

Nomenclature

A	area, m^2
C_p	specific heat at constant pressure, $J\,kg^{-1}\,K^{-1}$
C_{pr}	heat capacity of each cell matrix, $W\,K^{-1}$
ε	regenerator efficiency
M	mass of working gas in the engine, kg
$\dot{m}$	mass flow rate, $kg\,s^{-1}$
m	mass of gas in different component, kg
P	pressure, Pa
Q	heat, J
$\dot{Q}$	power, W
R	gas constant, $J\,kg\,K^{-1}$
T	temperature, K
U	convection heat transfer coefficient, $W\,m^{-2}\,K^{-1}$
V	volume, m^3
W	work, J

Subscripts

c	compression space
diss	dissipation
d	expansion space
E	entered
f	cooler
h	heater
irr	irreversible
p	loss
Pa	wall
r	regenerator
r_1	regenerator cell 1
r_2	regenerator cell 1
S	outlet
shtl	shuttle
T	total

indicated that the engine speed, engine torque and power output increase proportionally with a rise in the hot source temperature.

Walker [2] mentions other losses but without introducing them in the models: the conduction losses in the exchangers, the load losses, the shuttle losses and the gas spring hysteresis losses. Furthermore, these losses are not usually studied in literature because of their complexity. Urieli and Berchowitz [13] developed an adiabatic model and a quasi-stationary model where they introduced only the pressure drops into the exchangers. The results obtained by this model are better than those of the other models, but remain different from the experimental results. Hence, the Stirling engine performance depends on geometrical and physical parameters of the engine and on the working fluid gas properties such as regenerator efficiency and porosity, dead volume, swept volume, temperature of sources, pressure drop losses, shuttle losses, etc.

A dynamic model taking into account the different losses is developed by the authors and tested using the General Motor GPU-3 Stirling engine data, [14]. The results obtained proved better than those obtained by other models and correlate more closely with experimental data. The model is used to determine the losses in different engine compartments and to calculate the geometrical and physical parameters corresponding to minimal losses [15]. An optimization based on this model is presented in this article. It will help study the influence of geometrical and physical parameters on the prototype performance of a Stirling engine and therefore determine their optimal values.

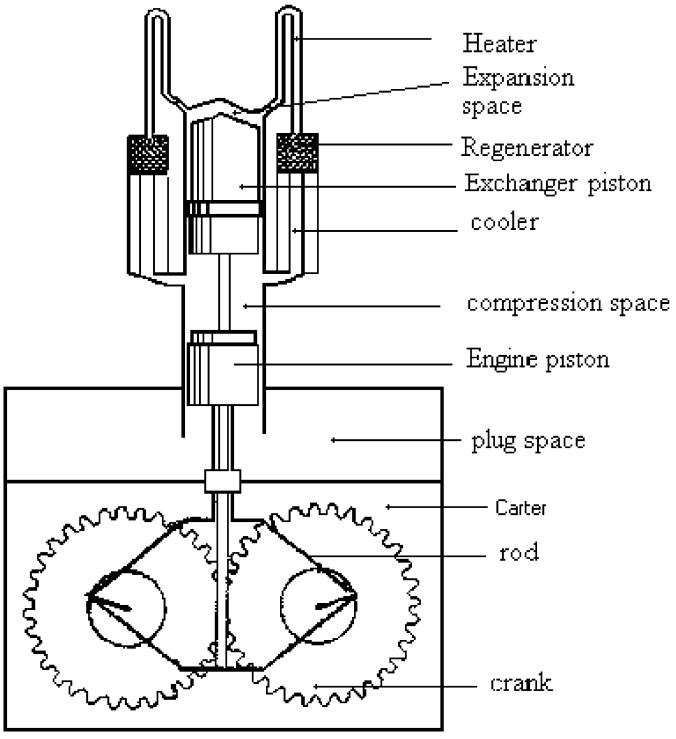

Fig. 1. Rhombic Stirling engine GPU-3 (built by General Motor [14]).

2. Dynamic model including losses

A second-order adiabatic model has been initially developed. The estimated values of the engine parameters are obtained and for the sake of validation, the results are compared with Berchowitz results under analogous conditions [14]. Afterward, a dynamic model, which takes into account the losses in the different engine elements, was developed.

The losses considered in this model are the energy dissipation by pressure drops in heat exchangers, energy lost due to internal conduction through the exchangers, energy lost due to external conduction in the regenerator, energy lost due to the shuttle effect in the displacer and energy lost due to gas spring hysteresis in the compression

and expansion spaces [14]. The mechanical friction between the moving parts is not considered.

The schematic model and the temperature distribution in the various engine components are shown in Fig. 2. The dynamic model of the developed Stirling engine is based on the following assumptions:

The gas temperature in the different engine elements is variable.
The cooler and the heater walls are maintained isothermal at temperatures T_{paf} and T_{pah}.
The gas temperature in the different components is calculated using the perfect gas law.
The regenerator is divided into two cells r1 and r2, each cell has been associated with its respective mixed mean gas temperature T_{r1} and T_{r2} expressed as follows:

$$T_{r1} = \frac{P_{r1} V_{r1}}{R m_{r1}}, \tag{1}$$

$$T_{r2} = \frac{P_{r2} V_{r2}}{R m_{r2}}. \tag{2}$$

An extrapolated linear curve is drawn through temperature values T_{r1} and T_{r2}, defining the regenerator interface temperature T_{f-r}, T_{r-r} and T_{r-h}, as follows [15]:

$$T_{f-r} = \frac{3T_{r1} - T_{r2}}{2}, \tag{3}$$

$$T_{r-r} = \frac{T_{r1} + T_{r2}}{2}, \tag{4}$$

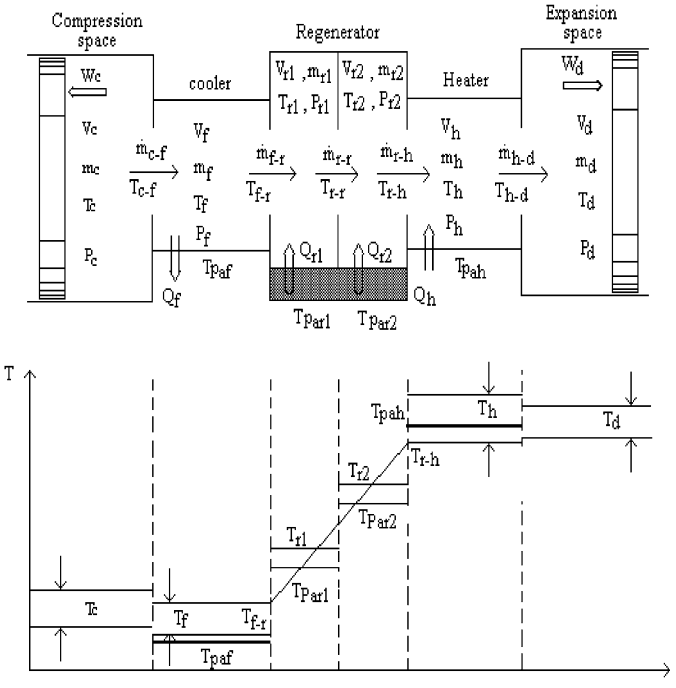

Fig. 2. Schematic model of the engine and various temperature distributions.

$$T_{r-h} = \frac{3T_{r2} - T_{r1}}{2}. \tag{5}$$

According to the flow direction of the fluid, the interface's temperatures are defined as follows [14]:

$T_{c-f} = T_c$ if $\dot{m}_{c-f} > 0$, otherwise $T_{c-f} = T_f$.

$T_{f-r} = T_f$ if $\dot{m}_{f-r} > 0$, otherwise $T_{f-r} = T_{r-r}$.

$T_{r-h} = T_{r-r}$ if $\dot{m}_{r-h} > 0$, otherwise $T_{r-h} = T_h$.

$T_{h-d} = T_h$ if $\dot{m}_{h-d} > 0$, otherwise $T_{h-d} = T_d$.

The regenerator matrix temperatures are therefore given by

$$\frac{dT_{par1}}{dt} = -\frac{\delta Q_{r1}}{C_{pr}\, dt}, \tag{6}$$

$$\frac{dT_{par2}}{dt} = -\frac{\delta Q_{r2}}{C_{pr}\, dt}. \tag{7}$$

Taking into account the losses by internal conduction in the exchangers: $\delta\dot{Q}_{pcdf}$, $\delta\dot{Q}_{pcdr1}$, $\delta\dot{Q}_{pcdr2}$, $\delta\dot{Q}_{pcdh}$ and external conduction in the regenerator, the power exchanged in the different heat exchangers are given by

$$\delta\dot{Q}_f = U_f A_{paf}(T_{paf} - T_f) - \delta\dot{Q}_{pcdf}, \tag{8}$$

$$\delta\dot{Q}_{r1} = \varepsilon U_{r1} A_{par1}(T_{par1} - T_{r1}) - \frac{\delta\dot{Q}_{pcdr1}}{2}, \tag{9}$$

$$\delta\dot{Q}_{r2} = \varepsilon U_{r2} A_{par2}(T_{par2} - T_{r2}) - \frac{\delta\dot{Q}_{pcdr2}}{2}, \tag{10}$$

$$\delta\dot{Q}_h = U_h A_{pah}(T_{pah} - T_h) - \delta\dot{Q}_{pcdh}, \tag{11}$$

where ε is the regenerator efficiency.

The heat transfer coefficient of exchanges U_f, U_{r1}, U_{r2} and U_h are available only empirically [13]. The total exchanged heat is

$$\delta\dot{Q} = \delta\dot{Q}_f + \delta\dot{Q}_{r1} + \delta\dot{Q}_{r2} + \delta\dot{Q}_h - \delta\dot{Q}_{pshtl}, \tag{12}$$

where $\delta\dot{Q}_{pshtl}$ is the shuttle loss in the displacer. Considering the loss due to gas spring hysteresis in the compression and expansion space: $\delta W_{irrc}/dt$ and $\delta W_{irrd}/dt$, evaluated in [14], the work done in a cycle is

$$\frac{\delta W}{dt} = P_c \frac{dV_c}{dt} + P_d \frac{dV_d}{dt} - \frac{\delta W_{irrc}}{dt} - \frac{\delta W_{irrd}}{dt}. \tag{13}$$

The total engine volume is

$$V_T = V_c + V_f + V_{r1} + V_{r2} + V_h + V_d. \tag{14}$$

Since there is a variable pressure distribution throughout the engine, the compression space pressure P_c has been arbitrarily chosen as the baseline pressure. At each increment of the solution, P_c is evaluated from the relevant differential equation and the pressure distribution is determined with respect to P_c.

The other variables of the dynamic model are given by the energy and mass conservation equation applied

to a generalized cell:

$$\delta\dot{Q} + C_p T_E \dot{m}_E - C_p T_S \dot{m}_S = P\frac{dV}{dt} + C_V \frac{d(mT)}{dt}, \quad (15)$$

$$M = m_d + m_c + m_f + m_r + m_h. \quad (16)$$

Applying the energy conservation equation to the different engine cells and including energy dissipation by pressure drop in the exchangers, $\delta\dot{Q}_{diss}$, and the other losses yields

$$-C_p T_{c-f}\dot{m}_{cS} = \frac{1}{R}\left(C_p P_c \frac{dV_c}{dt} + C_V V_c \frac{dP_c}{dt}\right) - \delta\dot{W}_{irrc}, \quad (17)$$

$$\delta\dot{Q}_f - \delta\dot{Q}_{dissf} + C_p T_{c-f}\dot{m}_{fE} - C_p T_{f-r}\dot{m}_{fS} = \frac{C_V V_f}{R}\frac{dP_c}{dt}, \quad (18)$$

$$\delta\dot{Q}_{r1} - \delta\dot{Q}_{dissr1} + C_p T_{f-r}\dot{m}_{r1E} - C_p T_{r-r}\dot{m}_{r1S} = \frac{C_V V_{r1}}{R}\frac{dP_c}{dt}, \quad (19)$$

$$\delta\dot{Q}_{r2} - \delta\dot{Q}_{dissr2} + C_p T_{r-r}\dot{m}_{r2E} - C_p T_{r-h}\dot{m}_{r2S} = \frac{C_V V_{r2}}{R}\frac{dP_c}{dt}, \quad (20)$$

$$\delta\dot{Q}_h - \delta\dot{Q}_{dissh} + C_p T_{r-h}\dot{m}_{hE} - C_p T_{h-e}\dot{m}_{hS} = \frac{C_V V_h}{R}\frac{dP_c}{dt}, \quad (21)$$

$$C_p T_{h-d}\dot{m}_d - \delta\dot{Q}_{pshtl} = \frac{1}{R}\left(C_p P_d \frac{dV_d}{dt} + C_V V_d \frac{dP_c}{dt}\right) - \delta\dot{W}_{irrd}. \quad (22)$$

Summing Eqs. (22)–(27), the pressure variation was obtained:

$$\frac{dP_c}{dt} = \frac{1}{C_v V_T}\left[R(\delta\dot{Q} - \delta\dot{Q}_{dissT}) - C_p\frac{\delta W}{dt}\right], \quad (23)$$

where $\delta\dot{Q}_{dissT} = \delta\dot{Q}_{dissf} + \delta\dot{Q}_{dissr1} + \delta\dot{Q}_{dissr2} + \delta\dot{Q}_{dissh}$, is the total heat dissipation generated by pressure drop.

The mass flow in the different engine components is given by the energy conservation equations (17)–(22):

$$\dot{m}_{cS} = -\frac{1}{RT_{c-f}}\left(P\frac{dV_c}{dt} + V_c\frac{dP_c}{\gamma\, dt}\right) + \frac{\delta\dot{W}_{irr}}{C_P T_{c-f}}, \quad (24)$$

$$\dot{m}_{fS} = \frac{1}{c_p T_{f-r}}\left(\delta\dot{Q}_f - \delta\dot{Q}_{dissf} + c_p T_{c-f}\dot{m}_{fE} - \frac{c_V V_f}{R}\frac{dP_c}{dt}\right), \quad (25)$$

$$\dot{m}_{r1S} = \frac{1}{c_p T_{r-r}}\left(\delta\dot{Q}_{r1} - \delta\dot{Q}_{dissr1} + c_p T_{f-r}\dot{m}_{r1E} - \frac{c_V V_{r1}}{R}\frac{dP_c}{dt}\right), \quad (26)$$

$$\dot{m}_{r2S} = \frac{1}{c_p T_{r-h}}\left(\delta\dot{Q}_{r2} - \delta\dot{Q}_{dissr2} + c_p T_{r-r}\dot{m}_{r2E} - \frac{c_V V_{r2}}{R}\frac{dP_c}{dt}\right), \quad (27)$$

$$\dot{m}_{hS} = \frac{1}{c_p T_{h-d}}\left(\delta\dot{Q}_h - \delta\dot{Q}_{dissh} + c_p T_{r-h}\dot{m}_{hE}\frac{dm_h}{dtE} - \frac{c_V V_h}{R}\frac{dP_c}{dt}\right), \quad (28)$$

with $\dot{m}_{cS} = \dot{m}_{fE}$, $\dot{m}_{fS} = \dot{m}_{r1E}$, $\dot{m}_{r1S} = \dot{m}_{r2E}$, $\dot{m}_{r2S} = \dot{m}_{hE}$ and $\dot{m}_{hS} = \dot{m}_{dE}$.

3. Prototype specifications

The developed model has been tested using data from the Stirling engine GPU-3 manufactured by General Motor; this engine has a rhombic motion transmission system, Fig. 1. The geometrical parameters of this engine are given in Table 1. The operating conditions are as follows: working gas helium at a mean pressure of 4.13 MPa, frequency 41.72 Hz, hot space temperature $T_{pah} = 977$ K and cold space temperature $T_{paf} = 288$ K. The measured power output was 3958 W, at a thermal efficiency of 35%. The independent differential equations, obtained in paragraph

Table 1
Geometric parameter values of the GPU-3 Stirling engine

Parameters	Values	Parameters	Values
Clearance volumes		Cooler	
Compression space	28.68 cm^3	Tubes number/cylinder	312
Expansion space	30.52 cm^3	Interns tube	1.08 mm
Swept volumes		Diameter	46.1 mm
Compression space	113.14 cm^3	Length of the tube	13.8 cm^3
Expansion space	120.82 cm^3	Void volume	
Exchanger piston conductivity	15 W/m K	Regenerator	
Exchanger piston stroke	46 mm	Diameter	22.6 mm
		Length	22.6 mm
Heater		Wire diameter	40 μm
Tubes number	40	Porosity	0.697
Tube inside diameter	3.02 mm	Units numbers/cylinder	8
Tube length	245.3 mm	Thermal conductivity	15 W/m K
Void volume	70.88 cm^3	Void volume	50.55 cm^3

2, are solved simultaneously for the variables: P_c, m_c, T_{r1}, W, etc.

The vector Y denotes the unknown functions. For example, Y_{pc} is the system gas pressure in the compression space. The initial conditions to be satisfied are noted:

$$Y(t_0) = Y_0.$$

The corresponding set of differential equations is expressed as

$$\frac{dY}{dt} = F(t, Y).$$

The objective is to find the unknown function $Y(t)$ which satisfies both the differential equations and the initial conditions. The system of equations is solved numerically using the classical fourth-order Runge–Kutta method, cycle after cycle until periodic conditions are reached.

To validate the numerical method used in the computation, the results are compared with those obtained by Urieli and Berchowitz [13] under the same conditions (adiabatic models) of the GPU-3 engine data. The comparison shows a good agreement [14].

4. Results of the dynamic model with losses

It should be noted that all losses have been included in the model; the heat flow rate for each component versus crank angle is illustrated in Fig. 3. The corresponding average power of the engine is equal to 4.27 kW. The average heat flow generated by the heater is equal to 10.8 kW; it yields an engine efficiency of 39.5. The power and the efficiency calculated by the model are very close to the power and the actual efficiency of the prototype given in paragraph 3.

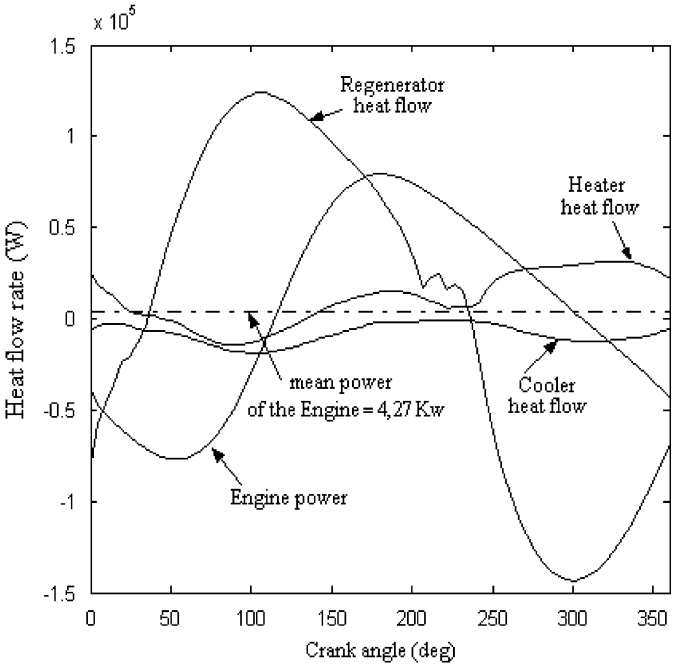

Fig. 3. Result of the dynamic model with losses.

The heat flow loss by internal conduction, the energy dissipation by pressure drop through the heat exchangers and the shuttle heat loss in the displacer are given in Fig. 4. The energy lost due to internal conduction is negligible in the heater and in the cooler and is about 8.5 kW in the regenerator, which represents 35% of the total energy loss. This is due to the lengthwise temperature variation, which is very significant in the regenerator. The energy lost due to dissipation is mainly observed in the regenerator; it reaches a maximum of 3.9 kW, with an average of 935 W. In the heater and in the cooler it is equal to 26.6 and 123 W, respectively. The average heat flow value lost by the shuttle

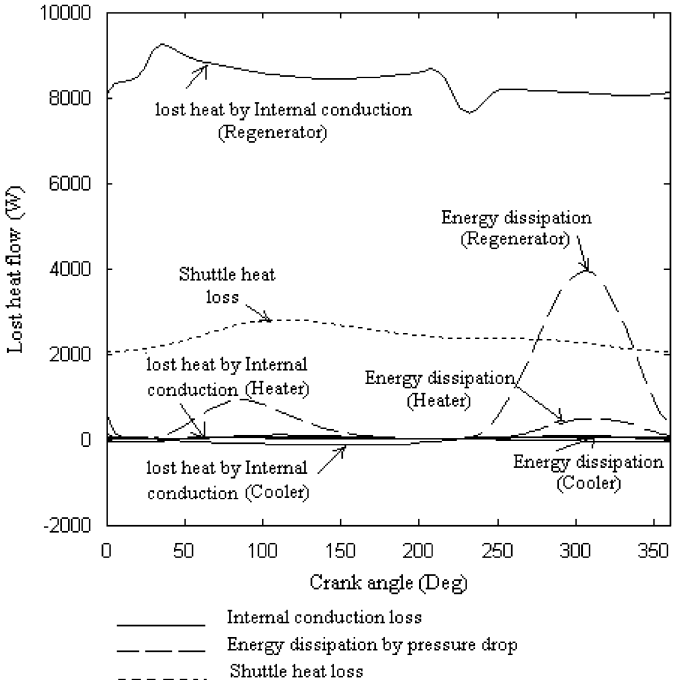

Fig. 4. Lost heat flow in the engine.

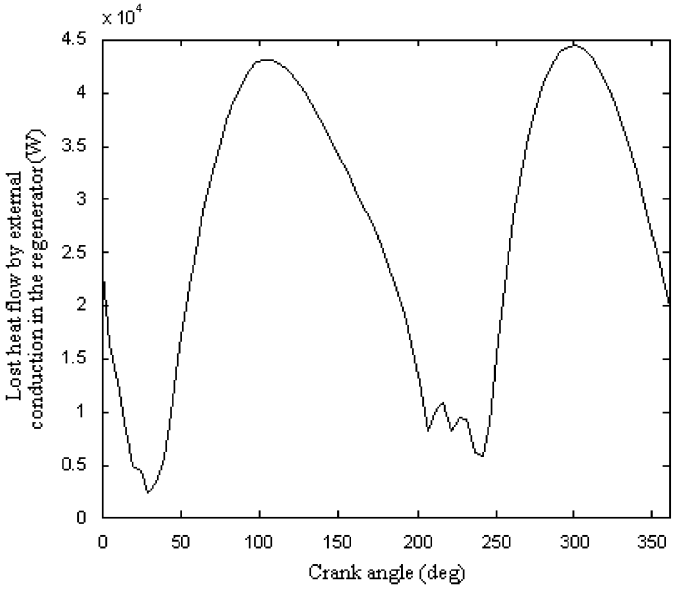

Fig. 5. Lost heat flow by external conduction in the regenerator.

effect is about 3.1 kW, which represents 13% of the total energy loss.

The energy lost due to external conduction in the regenerator is 27 kW, which represents 47% of the total losses (Fig. 5), and is very significant and depends mainly on the regenerator efficiency. The energy lost due to irreversibility in the compression and expansion spaces is very low [15].

5. Optimization of the Stirling engine performance

The energy losses occur mainly in the regenerator. They are primarily due to the losses by external and internal conduction and pressure drop through the heat exchangers. The energy lost due to the shuttle effect in the exchanger piston is also significant; it is about 13%. The other losses are very weak [15].

Reduction of these losses can improve the engine performance. Such losses depend mainly on the matrix conductivity of the regenerator, its porosity, the inlet temperature variation, the working gas mass, the regenerator volume and the geometrical characteristics of the displacer. To investigate the influence of these parameters on the prototype performance, we have varied the studied parameter in the model each time and have kept the others unchanged, equal to the prototype parameters.

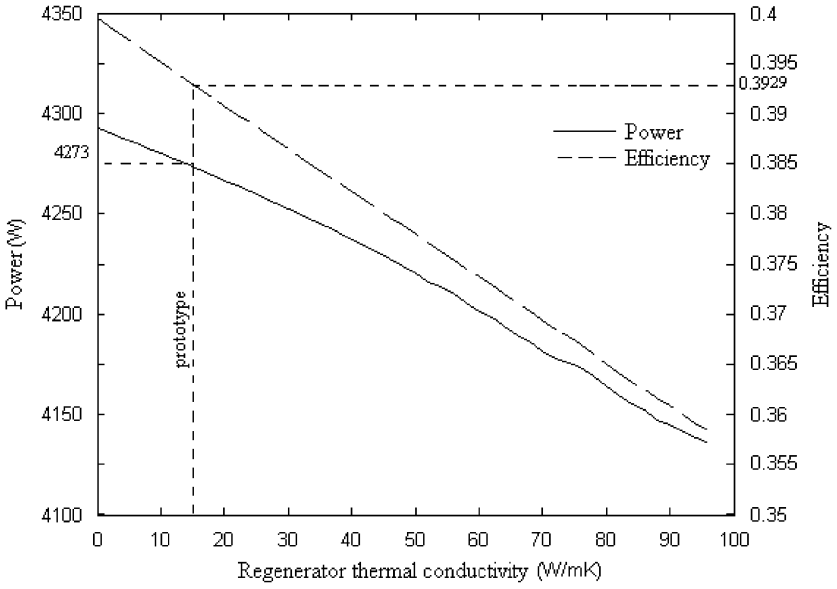

Fig. 6. Effect of regenerator thermal conductivity on performance.

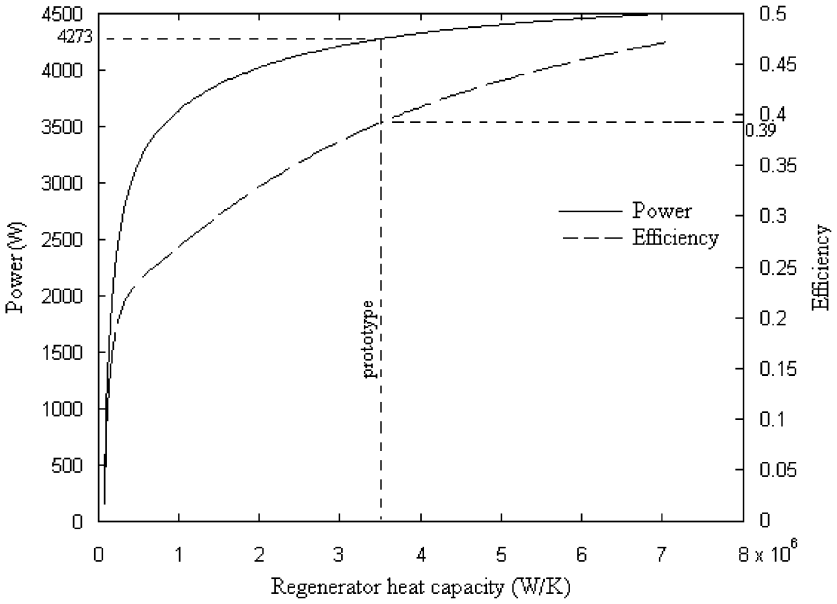

Fig. 7. Effect of regenerator heat capacity on performance.

5.1. Effect of the regenerator matrix conductivity and heat capacity

The performance of the engine depends on the conductivity and heat capacity of the material constituting the regenerator matrix. Fig. 6 shows that with an increase of the matrix regenerator thermal conductivity leads to a reduction of the performance due to an increase of internal conduction losses in the regenerator, [14,15]. Fig. 7 shows that the engine performance improves when the heat capacity of the regenerator matrix increases.

The matrix of the regenerator can be made from several materials. The performances of the engine are given according to the material type in Table 2. The performance of the engine depends on the regenerator matrix material. To increase heat exchange of the regenerator and to reduce the internal losses by conductivity, a material with high heat capacity and low conductivity must be chosen. Stainless steel and ordinary steel are the most suitable materials to prepare the regenerator matrix.

5.2. Effect of the regenerator porosity

The porosity of the regenerator is an important parameter for engine performance. It affects the hydraulic diameter, dead volume, velocity of the gas, regenerator heat transfer surface and regenerator effectiveness; and thus affects the losses due to external and internal conduction and the dissipation by pressure drop [15].

Engine performance decreases when the porosity increases due to an increase in the external conduction losses and a reduction of the exchanged energy between the gas and the regenerator, Q_r (Fig. 8). A low porosity will give a better result.

5.3. Effect of the regenerator temperature gradient (T_{f-r}–T_{r-h})

Although engine losses increase when the temperature gradient of the regenerator increases [15], the performance of the engine also increases (Fig. 9). In this case, the performance enhancement is due to an increase of the

Table 2
Effect of nature of the regenerator metal on the engine performance

Regenerator matrix metal	Volumetric capacity heat (J/m^3 K)	Conductivity (W/m K)	Engine power (W)	Engine effectiveness (%)	Exchanged energy in the regenerator (J)
Steel	3.8465×10^6	46	4258	38.84	441.25
Stainless steel	3.545×10^6	15	4273	39.29	448.72
Copper	3.3972×10^6	389	–	–	–
Brass	3.145×10^6	100	4080	34.6	415.67
Aluminum	2.322×10^6	200	3812	29.16	378.03
Granite	2.262×10^6	2.5	4091	34.51	430.75
Glass	2.1252×10^6	1.2	4062	33.85	427.8

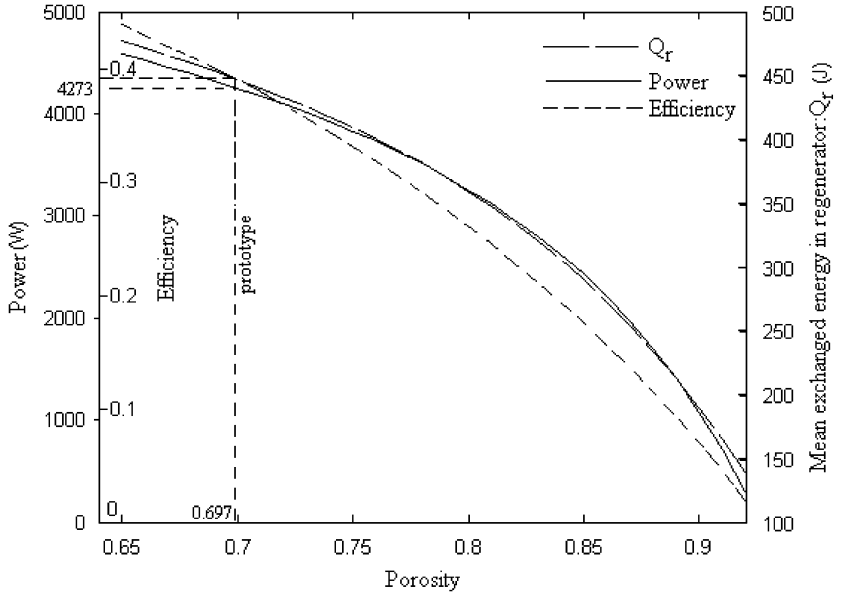

Fig. 8. Effect of regenerator porosity on performance and exchanged energy.

exchanged energy between the matrix and the working fluid of the regenerator.

5.4. Effect of the regenerator volume

To vary the regenerator volume, the diameter is fixed and the length is varied or vice versa. When the regenerator diameter is fixed at 0.0226 m, the length affects the performance. Although the energy exchanged increases, the engine power and efficiency reach a maximum. At a length equal to 0.01 m, then, the power decreases quickly, as shown in Fig. 10. This can be explained by an increase of the dead volume.

When the regenerator length is constant and $L = 0.022$ m, the performance decreases when the regenerator diameter increases (Fig. 11). The dead volume and the exchanged energy in the regenerator also decrease.

5.5. Effect of the fluid mass

An increase of the total mass of gas in the engine leads to an increase in the density, mass flow, gas velocity, load and function pressure. Therefore, the increase in the total mass of gas in the engine leads to more energy loss by pressure drop [15]; however, the engine power increases and the efficiency reaches a maximum of about 40% when the mass

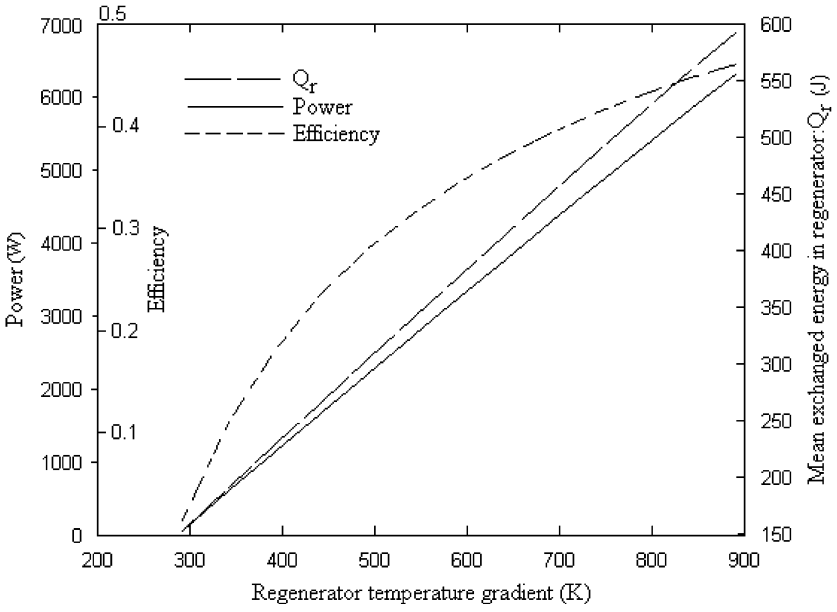

Fig. 9. Effect of regenerator temperature gradient on performance.

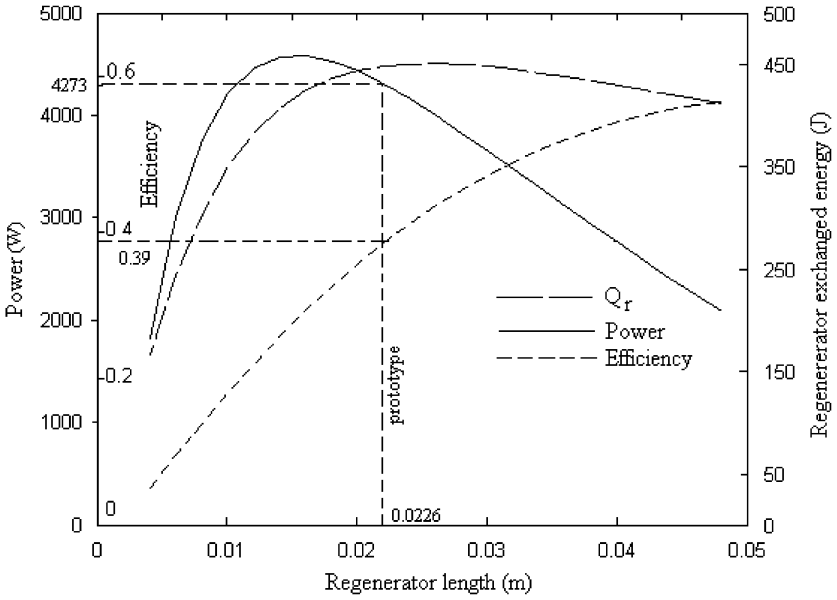

Fig. 10. Effect of regenerator length on performance and exchanged energy.

is equal to 0.8 g (Fig. 12). When the mass increases further, the decrease of the efficiency is due to an increase of the pressure loss and the limitation of the heat exchange capacity in the regenerator and the heater. The use of a mass of gas equal to 1.5 g in the engine leads to an acceptable output and a higher power than in the prototype.

5.6. Effect of expansion volume and exchanger piston conductivity

The expansion volume and the exchanger piston conductivity considerably affect the losses due to the shuttle effect, which represents 13% of the engine total losses. To vary the expansion volume, the stroke constant can be maintained and the piston surface can be varied or vice versa. When the piston stroke is constant and equal to the prototype value of 0.046 m, the effect of the piston surface on the performance is given in Fig. 13. When the section increases, the engine power increases, but the efficiency reaches a maximum. If the exchanger piston area is equal to 0.0045 m^2, a power higher than 5 kW and an output slightly lower than that of the prototype can be reached. When the exchanger piston area is constant and equal to the prototype value of 0.0038 m^2, the effect of the stroke variation on the performance is given in Fig. 14.

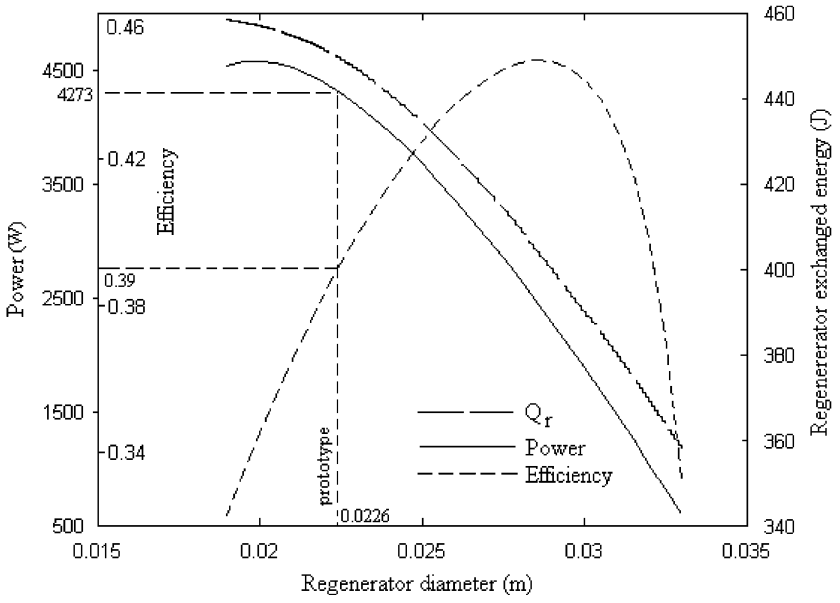

Fig. 11. Effect of regenerator diameter on performance and exchanged energy.

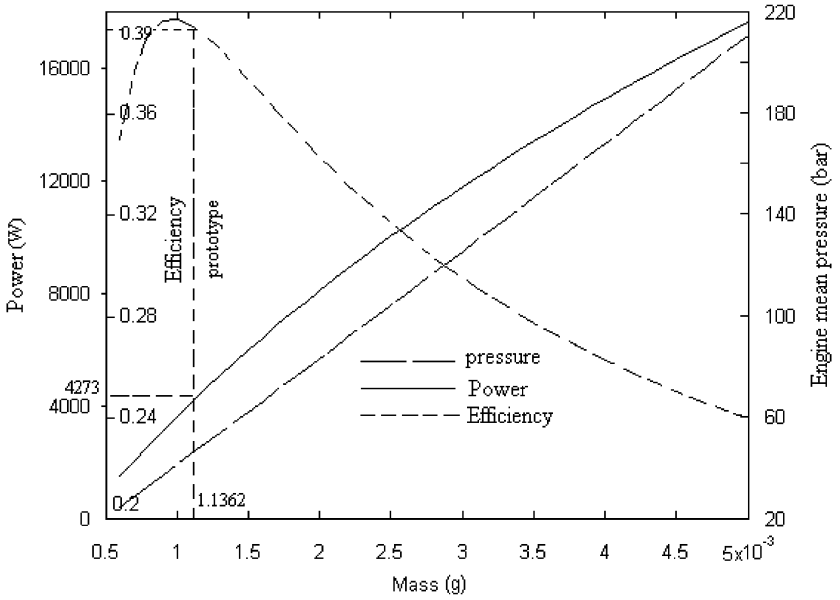

Fig. 12. Effect of fluid mass on performance and engine mean pressure

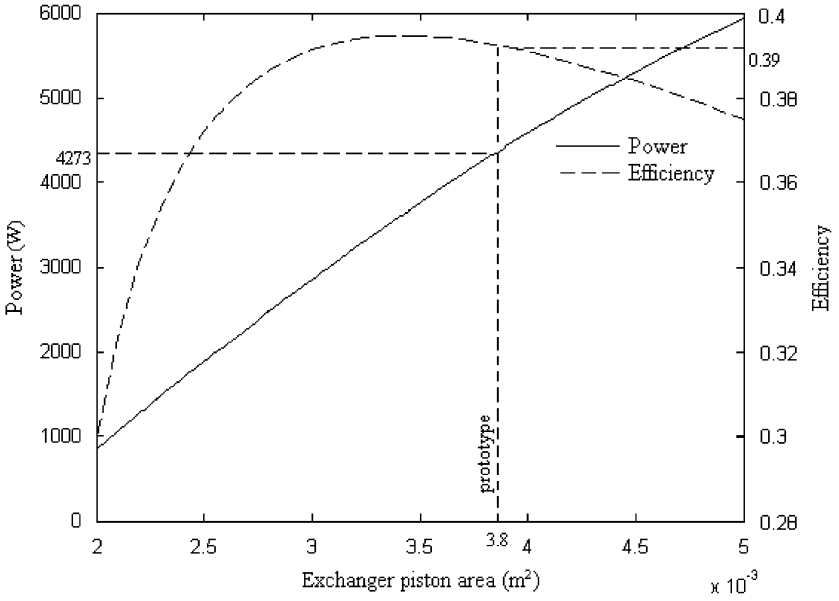

Fig. 13. Effect of exchanger piston area on engine performance.

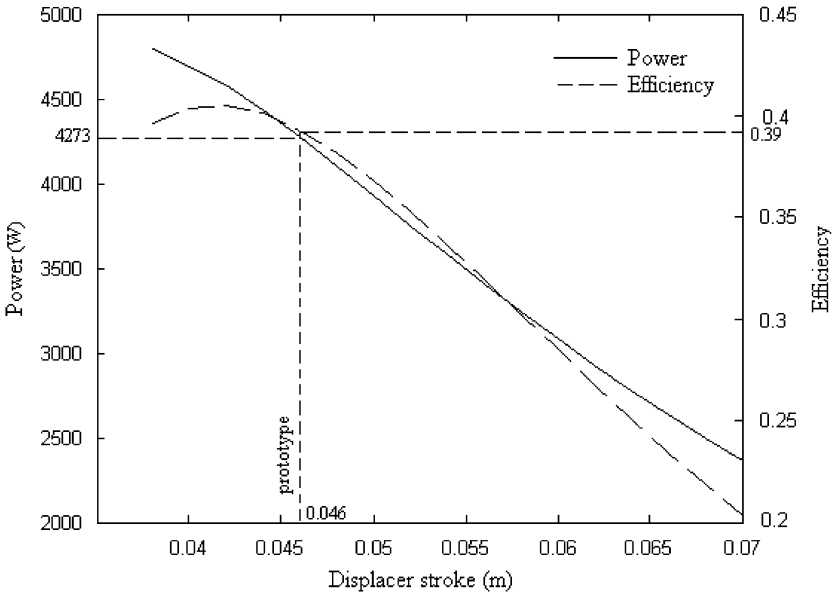

Fig. 14. Effect of exchanger piston stroke on engine performance.

When the stroke increases, the engine power decreases, but the efficiency reaches a maximum. The optimal performances are superior to that of the prototype. They are obtained when the area and the stroke are, respectively, equal to $3.8\,10^{-3}\,m^2$ and 0.042 m, which correspond to a power of 4500 W and an efficiency of 41%.

The thermal conductivity of the exchanging piston considerably affects the engine performances (Fig. 15). A weak conductivity reduces the losses due to the shuttle effect and consequently increases the engine power and the efficiency.

6. Conclusion

The Stirling engine prototypes designed have low outputs because of the considerable losses in the regenerator and the exchanger piston. These losses are primarily due to external and internal conduction, pressure drops in the regenerator and shuttle effect in the exchanger piston, which depend on the geometrical and physical parameters of the prototype design. An optimization of these parameters has been carried out using the GPU-3 engine data, and has led to a reduction of the losses and to a notable

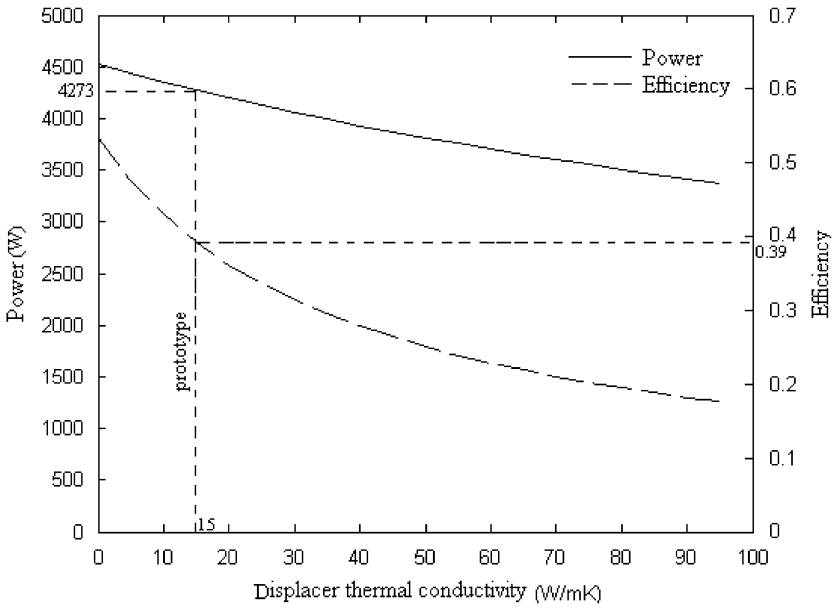

Fig. 15. Effect of displacer thermal conductivity on performance.

improvement in the engine performance. The parameters of this prototype were first applied on the developed model; the results were very close to the experimental data. Then, the influence of each geometrical and physical parameter on the engine performance and the exchanged energy of the regenerator was studied.

A reduction of the matrix porosity and conductivity of the regenerator increase the performance. A rise of the total mass of gas leads to an increase of the engine power and function pressure; however, the efficiency reached a maximum. When the displacer section increases and the piston stroke decreases, the engine power increases, and the efficiency attains a maximum. A low conductivity of the exchanger piston reduces the losses due to the shuttle effect and consequently increases the engine power and efficiency.

In future, it is hoped to introduce simultaneously in the model all the optimal parameters obtained, determine the optimal design parameters and consequently the interesting performance.

References

[1] Stouffs P. Machines thermiques non conventionnelles: état de l'art, applications, problèmes à résoudre…, Thermodynamique des machines thermiques non conventionnelles, Journée d'étude du 14 octobre 1999, SFT, Paris.

[2] Walker G. Stirling engines. Oxford: Clarendon Press; 1980.

[3] Kolin I. Stirling motor: history–theory–practice. Dubrovnik: Inter University Center; 1991.

[4] Timoumi Y, Ben Nasrallah S. Design and fabrication of a Stirling–Ringbom engine running at a low temperature. In: Proceedings of the TSS International conference in mechanics and engineering, ICAME, March 2002, Hammamet-Tunisia.

[5] Halit K, Huseyin S, Atilla K. Manufacturing and testing of a V-type Stirling engine. Turk J Engine Environ Sci 2000;24:71–80.

[6] Popescu G, Radcenco V, Costea M, Feidt M. Optimisation thermodynamique en temps fini du moteur de Stirling endo- et exo-irréversible. Rev Gén Therm 1996;35:656–61.

[7] Kaushik SC, Kumar S. Finite time thermodynamic analysis of endoreversible Stirling heat engine with regenerative losses. Energy 2000;25:989–1003.

[8] Wu F, Chen L, Wu C, Sun F. Optimum performance of irreversible Stirling engine with imperfect regeneration. Energy Convers Manage 1998;39:727–32.

[9] Kongtragool B, Wongwises S. Thermodynamic analysis of a Stirling engine including dead volumes of hot space, cold space and regenerator. Renew Energy 2006;31:345–59.

[10] Costa M, Petrescu S, Harman C. The effect of irreversibilities on solar Stirling engine cycle performance. Energy Convers Manage 1999;40:1723–31.

[11] Cun-quan Z, Yi-nong W, Guo-lin J. Dynamic simulation of one-stage Oxford split-Stirling cryocooler and comparison with experiment. Cryogenics 2002;42:377–586.

[12] Cinar C, Yucesu S, Topgul T, Okur M. Beta-type Stirling engine operating at atmospheric pressure. Appl Energy 2005;81: 351–7.

[13] Urieli I, Berchowitz D. Stirling cycle engine analysis. Bristol: Adam Hilger Ltd.; 1984.

[14] Tlili I, Timoumi Y, Ben Nasrallah S. Numerical simulation and losses analysis in a Stirling engine. Heat Technol 2006;24:97–105.

[15] Timoumi Y, Tlili I, Ben Nasrallah S. Reduction of energy losses in a Stirling engine. Heat Technol 2007; 27(1), in press.